AIAA 80-1395R

# Prediction and Measurement of Incompressible Turbulent Aerodynamic Trailing Edge Flows

A. J. Baker*
*University of Tennessee, Knoxville, Tenn.*
J. C. Yu†
*NASA Langley Research Center, Hampton, Va.*
J. A. Orzechowski‡
*Computational Mechanics Consultants, Inc., Knoxville, Tenn.*
and
T. B. Gatski§
*NASA Langley Research Center, Hampton, Va.*

**A viscous-inviscid interaction algorithm is developed for prediction of two-dimensional mean and fluctuating velocity distributions in the wake immediately downstream of an airfoil trailing edge. A composite pressure field is defined, and a Poisson equation solved for transverse pressure distributions. A parabolized form of the time-averaged steady Navier-Stokes equations is solved in conjunction with a viscous-augmented, two-dimensional potential flow analysis. A tensor constitutive equation predicts Reynolds stress distributions from solutions of a turbulence kinetic energy two equation closure model. Numerical predictions compare favorably with experimental data for mean and fluctuating velocities, and Reynolds shear stress distributions, in the trailing edge wake of a NACA 63-012 airfoil.**

## Introduction

TURBULENT boundary-layer flows departing an aerodynamic trailing edge are verified strong acoustic sources. Alteration of the aerodynamic surface can alter far-field intensity by local absorbtion as well as modifying flow structure prior to departing the trailing edge. The technical requirement is to predict accurately the nearfield evolution of mean and fluctuating velocity fields immediately upon departure from the trailing edge. The concurrent requirement is to assess factors influencing flow evolution, and to compare results to quality experimental data.

The time-averaged steady flow Navier-Stokes equations are assumed to adequately describe the flow, and several simplified forms have been used for turbulent wake flow numerical simulations. Prediction of the two-dimensional turbulent near wake of a symmetrical airfoil is documented[1] using the shear layer equations and an eddy viscosity hypothesis. Refinement of the method, including use of Goldstein variables and a double-structured box numerical procedure, while retaining use of eddy viscosity is recently reported.[2] A procedure alternative to direct solution of the shear layer equations employs an asymptotic analysis and definition of a triple deck structure[3] including turbulent flows.[4]

This paper presents an analysis yielding sets of partial differential equations for prediction of turbulent aerodynamic wake flowfields. It is the generalization of a procedure developed for slot jet flows downstream of sharp edged planar flaps.[5] The equation systems are embedded within an iterative, viscous-inviscid interaction algorithm, and the procedure is applicable to nonseparated, subsonic two-dimensional airfoil wake flows including angle of attack. A key element is identification of a Reynolds stress constitutive equation which permits determination of stress components in terms of solution variables. Coupled with a low turbulence Reynolds number model, to allow solution of all variables through the near-surface sublayer, this procedure admits prediction of detailed distributions of mean velocity and fluctuating velocity correlations in the near wake.

Table 1 summarizes the basic elements of the interaction algorithm solution sequence. Phase A serves to define the

**Table 1 Aerodynamic viscous-inviscid interaction algorithm**

| Phase | | Description of sequence | |
|---|---|---|---|
| A | Input | 1) | Problem specified by $M_\infty$, $C$, $t/C$, $\alpha$, $Re$[a] |
| B | Viscous-corrected potential (2DPHI) | 1) | Solve $\nabla^2\phi = 0$ on basic airfoil and wake centerline |
| | | 2) | Solve integral boundary-layer equation for $\delta^*$ |
| | | 3) | Extrapolate $\delta^*$ onto wake |
| | | 4) | Repeat B 1-3 until $\delta^*(x_1)$ stationary |
| C | Turbulent boundary layer (2DBL) | 1) | Initialize $\bar{u}_1(x_2)$ from data or Cole's law across $\delta(x_1)$ at $x_1/C \approx 0.9$ |
| | | 2) | Initialize $k(x_2)$ and $\epsilon(x_2)$ using self-generation procedure or data |
| | | 3) | Execute 2DBL on $0.9 \le x_1/C \le 1.0$ using phase B $C_p$ |
| D | Parabolic Navier-Stokes (2DPNS) | 1) | Initialize 2DPNS at $x_1/C = 1.0$ using 2DBL solution |
| | | 2) | Execute 2DPNS on $1.0 < x_1/C < 1.1$ using phase B $C_p$ |
| | | 3) | Modify 2DPHI boundary conditions, using 2DBL/2DPNS solution for $\bar{u}_2$ "onset" velocity |
| | | 4) | Recompute 2DPHI to refine $C_p$ distribution |
| | | 5) | Repeat phase B-D until $C_p$ stationary |

[a] $M_\infty$ = Mach number, $C$ = chord, $t/C$ = thickness distribution, $\alpha$ = angle of attack, $Re$ = Reynolds number.

Presented as Paper 80-1395 at the AIAA 13th Fluid and Plasma Dynamics Conference, Snowmass, Colo., July 14-16, 1980; submitted Sept. 18, 1980; revision received June 8, 1981. 

*Professor of Engineering Science and Mechanics. Associate Fellow AIAA.
†Aerospace Technologist, Acoustics & Noise Reduction Division. Member AIAA.
‡Principal Consultant.
§Research Scientist, Acoustics & Noise Reduction Division.

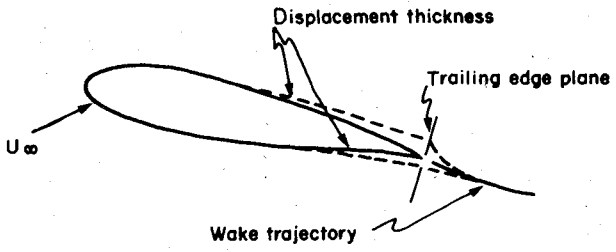


**Fig. 1 Schematic of viscous-corrected potential solution.**

geometric and flow parameters. Phase B is an inexpensive iterative sequence, wherein the Laplacian for perturbation potential function $\phi$ (2DPHI) is solved repeatedly on the airfoil and wake displacement thickness distribution $\delta^*$. Upon convergence, this potential solution provides the initial estimate of the inviscid flow pressure boundary conditions for the following phases.

In phases C and D, the complete two-dimensional boundary layer (2DBL) and parabolic Navier-Stokes (2DPNS) equation systems, including the two-equation turbulence closure equations, are solved upstream and downstream of the trailing edge. These solutions yield detailed distributions of the mean velocity, and fluctuating velocity correlations, as well as the computed distribution of efflux velocity $\bar{u}_2(x_1)$ from the vorticity-dominated domain. The 2DPHI solution from phase B is repeated, using this velocity determination as the "onset" velocity boundary condition specification. This yields a refined inviscid flow pressure field boundary condition for phases C and D. The sequence of 2DBL, 2DPNS, and 2DPHI solutions is repeated as necessary to yield a unique determination for the coupling pressure distribution.

The description of the appropriate differential equation systems and the turbulence closure model is presented. A finite element penalty-constrained numerical algorithm is identified. The viscous-inviscid interaction algorithm is employed to predict the trailing-edge wake flow for a NACA 63-012 airfoil and compared to detailed experimental data for the case of 0-deg angle of attack. Factors affecting profile evolution are identified, and the numerical predictions include angle of attack.

## Problem Description

### Viscous-Corrected Potential Flow

For the phase B solution, the computational domain is a "sufficiently" large region surrounding the airfoil and the wake trajectory, that become augmented in thickness distribution by a viscous correction, see Fig. 1. The Laplacian for perturbation potential function $\phi$ is solved on this domain subject to the onset flow boundary condition,

$$l(\phi)=\frac{\partial\phi}{\partial x_i}\hat{n}_i-[U_\infty\hat{\epsilon}_i-u_i]\hat{n}_i=0 \tag{1}$$

where $\hat{\epsilon}_i$ is the unit vector corresponding to angle of attack, $u_i$ is the local velocity vector, and the tensor index summation convention is inferred. The solution for $\phi$ yields determination of the inviscid flow pressure distribution $C_p(x_1)$ on the estimated airfoil and wake thickness distribution. The integral momentum boundary-layer equation[6] is solved, using this $C_p$, yielding an estimated turbulent boundary layer and wake displacement thickness distribution $\delta^*(x_1)$. These data are used to redefine the estimated airfoil and wake unit normal distribution $\hat{n}_i(x)$, Eq. (1), and the solution sequence repeated to convergence of $C_p(x_1)$. A detailed discussion of this procedure is given in Ref. 7.

### Parabolic Turbulent Flow

The equation systems governing the turbulent flow regions are simplifications of the steady time-averaged Navier-Stokes equations. For a persistent mean flow direction, i.e., no separation, the parabolic approximation results from assuming chordwise diffusion effects are negligible. The overall elliptic coupling is returned through the inviscid pressure coefficient interaction. The resultant "parabolic" Navier-Stokes equations for an incompressible fluid are

$$L(\bar{p}_0)=\frac{\partial\bar{u}_1}{\partial x_1}+\frac{\partial\bar{u}_2}{\partial x_2}=0 \tag{2}$$

$$L(\bar{u}_1)=\frac{\partial}{\partial x_1}[\bar{u}_1\bar{u}_1+\overline{u_1'u_1'}]+\frac{\partial}{\partial x_2}[\bar{u}_1\bar{u}_2+\overline{u_1'u_2'}]+\frac{1}{\rho}\frac{\partial\bar{p}}{\partial x_1}-\frac{\nu}{Re}\frac{\partial^2\bar{u}_1}{\partial x_2^2}=0 \tag{3}$$

$$L(\bar{u}_2)=\frac{\partial}{\partial x_1}[\bar{u}_1\bar{u}_2+\overline{u_1'u_2'}]+\frac{\partial}{\partial x_2}[\bar{u}_2\bar{u}_2+\overline{u_2'u_2'}]+\frac{1}{\rho}\frac{\partial\bar{p}}{\partial x_2}-\frac{\nu}{Re}\frac{\partial^2\bar{u}_2}{\partial x_2^2}=0 \tag{4}$$

$$L(k)=\frac{\partial}{\partial x_1}[\bar{u}_1k]+\frac{\partial}{\partial x_2}[\bar{u}_2k]+\overline{u_i'u_j'}\frac{\partial\bar{u}_j}{\partial x_i}+\epsilon-\frac{\nu}{Re}\frac{\partial^2k}{\partial x_2^2}-\frac{\partial}{\partial x_i}\left[C_k\overline{u_i'u_j'}\frac{k}{\epsilon}\frac{\partial k}{\partial x_j}\right]=0 \tag{5}$$

$$L(\epsilon)=\frac{\partial}{\partial x_1}[\bar{u}_1\epsilon]+\frac{\partial}{\partial x_2}[\bar{u}_2\epsilon]+C_\epsilon'\overline{u_i'u_j'}\frac{\epsilon}{k}\frac{\partial\bar{u}_i}{\partial x_j}+C_\epsilon^2\frac{\epsilon^2}{k}-\frac{\partial}{\partial x_i}\left[C_\epsilon\overline{u_i'u_j'}\frac{k}{\epsilon}\frac{\partial\epsilon}{\partial x_j}\right]=0 \tag{6}$$

The variables in Eqs. (2-6) are nondimensionalized by the reference velocity and viscosity scales $U_\infty$ and $\nu_\infty$, and $Re\equiv U_\infty L/\nu_\infty$. The overbar denotes time-average, the prime indicates fluctuation about the mean, and the tensor indices sum $1\le(i,j)\le2$. The turbulence kinetic energy $k$ is

$$k\equiv\tfrac{1}{2}\overline{u_i'u_i'} \tag{7}$$

and the isotropic turbulence dissipation function $\epsilon$ is defined as

$$\epsilon\delta_{ij}=2\bar{\nu}\,\overline{\frac{\partial u_i'\partial u_j'}{\partial x_k\partial x_k}} \tag{8}$$

For the boundary-layer (2DBL) solutions upstream of the trailing-edge terminus, Eq. (2) is solved directly for $\bar{u}_2$. The boundary-layer order of magnitude analysis, assuming $\overline{u_i'u_j'}\approx0(\bar{u}_2)$, shows $\overline{u_1'u_1'}$ negligible in Eq. (3). Balancing the lowest order terms in Eq. (9) produces the transverse pressure distribution.

$$\frac{\partial}{\partial x_2}[\bar{p}+\overline{\rho u_2'u_2'}]=0 \tag{9}$$

Equation (9) is also valid well downstream of the trailing edge. However, in the immediate downstream wake, the large induced flowfield accelerations render the elementary order of magnitude analysis invalid. The necessary generalization is achieved by casting Eq. (4) as a Poisson equation for pressure. Differentiating on $x_2$, and assuming convection and laminar viscosity effects remain higher order, yields

$$L(\bar{p})=\frac{1}{\bar{\rho}_0}\frac{\partial^2\bar{p}}{\partial x_2^2}+\frac{\partial}{\partial x_2}\left[\frac{\partial\overline{u_1'u_2'}}{\partial x_i}\right]=0 \tag{10}$$

The solution of a linear Poisson equation is constituted of complementary and particular parts. The complementary field $p_c$ is the solution to the homogeneous equation with specified boundary conditions. These are determined from the viscous-corrected inviscid $C_p(x_1)$ distribution, as estimated by the phase B solution. In two-dimensional flow, therefore, the

complementary pressure distribution is the linear interpolate of the freestream values. The particular pressure $p_p$ is the solution to Eq. (10) that vanishes at the end points where $p_c$ is known. Hence, the 2DPNS pressure distribution is the composite solution

$$\bar{p}(x_i) = p_c(x_i) + p_p(x_i) \tag{11}$$

which must converge to a unique solution during iteration through the viscous-inviscid interaction algorithm. Since derivatives in the downstream direction are involved in the solution for $p_p$, the influence of the gradient of $p_p$ in the $\bar{u}_1$ momentum equation is retarded by one interaction iteration cycle.

#### Reynolds Stress Closure

Equations (3-10) require determination of the kinematic Reynolds stress $-\overline{u_i'u_j'}$. The primary output of the numerical solution is the detailed distribution in the near wake region. Rather than numerically solving the corresponding Reynolds stress transport equations, this study has utilized a tensor constitutive equation.[8] The first three terms in the tensor field expansion are determined of the form

$$\overline{u_i'u_j'} = \alpha_1 \overline{u_k'u_k'}\alpha_{ij} + \alpha_2 e_{ij} + \alpha_3 e_{ik}e_{kj} + \ldots \tag{12}$$

where $e_{ij}$ is the symmetric mean velocity strain rate tensor. The expansion coefficients $\alpha_i$ are determined using a parabolic order of magnitude analysis.[9] The final form for the aerodynamic wake configuration, retaining both first- and second-order terms,[7] and using Eq. (2), is

$$\overline{u_1'u_1'} = C_1 k - C_2 C_4 \frac{k^3}{\epsilon^2}\left[\frac{\partial \bar{u}_1}{\partial x_2}\right]^2 + 2C_4 \frac{k^2}{\epsilon}\frac{\partial \bar{u}_2}{\partial x_2}$$

$$\overline{u_2'u_2'} = C_3 k - C_2 C_4 \frac{k^3}{\epsilon^2}\left[\frac{\partial \bar{u}_1}{\partial x_2}\right]^2 - 2C_4 \frac{k^2}{\epsilon}\frac{\partial \bar{u}_2}{\partial x_2}$$

$$\overline{u_3'u_3'} = C_3 k$$

$$\overline{u_1'u_2'} = -C_4 \frac{k^2}{\epsilon}\frac{\partial \bar{u}_1}{\partial x_2} \tag{13}$$

By definition for two-dimensional flows, $\overline{u_1'u_3'} = 0 = \overline{u_2'u_3'}$. The expansion coefficients $C_i$ are[10]

$$C_1 \equiv \frac{22(C_{01}-1) - 6(4C_{02}-5)}{33(C_{01}-2C_{02})}$$

$$C_2 \equiv \frac{4(3C_{02}-1)}{11(C_{01}-2C_{02})}$$

$$C_3 \equiv \frac{22(C_{01}-1) - 12(3C_{02}-1)}{33(C_{01}-2C_{02})}$$

$$C_4 \equiv \frac{44C_{01} - 22C_{01}C_{02} - 128C_{02} - 36C_{02}^2 + 10}{165(C_{01}-2C_{02})^2} \tag{14}$$

The suggested values[11] of the "universal" empirical constants are $C_{01} = 2.8$ and $C_{02} = 0.45$.

The stress closure equation must be modified near the airfoil surface to account for the low turbulence Reynolds number in the sublayer structure. This is accomplished using an exponential damping function $\omega$ to modify the turbulence dissipation length scale $l_d$ in the form

$$l_d \equiv \omega^\beta C_4 (k^{3/2}/\epsilon) \tag{15}$$

where $\beta > 0$ is a parameter to be determined. The damping function $\omega$ is defined, using the concept of Van Driest damping,[6] as

$$\omega = [1 - \exp(-\alpha Re_t)] \tag{16}$$

The turbulence Reynolds number $Re_t$ is evaluated using the shear velocity ($u_\tau$) and normal distance to the surface, $Re_t \equiv u_\tau x_2/\nu$. The parameter $\alpha > 0$ adjusts the damping decay rate. The expression for shear stress $\overline{u_1'u_2'}$, Eq. (13) defines (as well) the kinematic eddy viscosity $\nu^t \equiv k^{1/2} l_d$. Therefore, by comparison, the Reynolds stress model is adjusted for low turbulence levels by the definition $C_4 \Rightarrow \omega^\beta C_4$. Correspondingly, it was assumed that all $C_i \Rightarrow \omega^\beta C_i$, $1 \le i \le 4$, in Eq. (13).

With this modification, Eq. (13) provides the required Reynolds stress closure. Importantly, the equations governing $k$ and $\epsilon$, Eqs. (5) and (6), can be integrated through the sublayer to the airfoil surface with no model constant adjustment. This is imperative for the analysis, since the dominant action immediately downstream of the trailing edge is essentially confined to this region previously dominated by existence of the aerodynamic surface. Correspondingly, the airfoil surface boundary conditions for a 2DBL solution are all variables vanishing. All dependent variables merge into the freestream with vanishing normal derivative. This freestream boundary condition also remains valid for $\bar{u}_1$, $k$, and $\epsilon$ for the 2DPNS solution in the wake. The continuity equation, Eq. (2), provides the freestream Neumann constraint for $\bar{u}_2$. The 2DPNS solution domain span is nominally double that of the 2DBL solution, thus placing the surface-dominated flow region into the center of the wake flow domain. The initial conditions required to start the 2DBL solution of Eqs. (2), (3), (5), and (6) are established using experimental data, if available, or self-generation techniques based upon boundary layer and mixing length concepts. The 2DBL solution at the trailing edge provides the initial condition for the 2DPNS wake solution.

## Numerical Solution Algorithm

The phase B viscous-corrected potential flow solutions are computed using a production finite-element code. The 2DBL solutions of Eqs. (2), (3), (5), and (6) are generated using an implicit, dissipative finite-element algorithm.[12] The 2DPNS algorithm for Eqs. (2-6) employs the same implicit procedure, with addition of a measure of the continuity equation solution as a penalty differential constraint on the momentum equation, Eq. (2). For both the 2DBL/2DPNS solutions, the finite-element discretization spans the $x_2$ coordinate direction, and the solution domain extends to well outside the boundary layer/wake edge. The 2DBL/2DPNS equation systems are marched downstream parallel to the $x_1$ direction.

A description of the 2DBL algorithm, including accuracy and convergence, is given in Refs. 13 and 14. The 2DPNS algorithm concept is described in Ref. 12. For both equation sets, the vector approximate solution $q_i^h(x_j) \equiv \{\bar{u}_1, \bar{u}_2, k, \epsilon\}$, is constructed using a finite dimensional subspace of $H_0^1$, the Hilbert space of all functions possessing square integrable first derivatives and satisfying the boundary conditions. The space of piecewise continuous linear polynomials on $x_2$ was chosen, defined on disjoint interior finite-element domains, the union of which forms the discretization. Hence,

$$q_i(x_j) \approx q_i^h(x_j) \equiv \sum_{e=1}^{M} q_i^e(x_j) \tag{17}$$

where the elemental approximation is

$$q_i^e(x_i) \equiv \{N_k(x_2)\}^T \{QI(x_1)\}_e \tag{18}$$

The sub- or superscript $e$ denotes pertaining to the $e$th finite element, $\Omega_e \equiv x_2^0 x x_1$, and the elements of the row matrix $\{N_k(x_2)\}^T$ are linear ($k = 1$) polynomials forming a cardinal basis.[14]

The functional requirement of the algorithm is to render the error in $q_i^h$ minimum in some norm. This is accomplished within the finite-element algorithm by requiring the error in Eqs. (2-6), i.e., $L(q_i^h)$ to be orthogonal to the elements of $\{N_k\}$ employed to define $q_i^h$. Nonlinearly induced instabilities are controlled, for the dissipation equation [Eq. (6)] only, by requiring that error in $\nabla L(q_i^h)$ also be orthogonal to $\{N_k\}$. Finally, for the 2DPNS algorithm statement, the measure of the error in Eq. (2) is applied as a differential constraint penalizing the solution of Eqs. (3-6).

Identifying the (Lagrange) multiplier set $\beta_l$, the three independent constraints are combined linearly to form the theoretical statement of the finite-element algorithm.

$$\int \{N_k\} L(q_i^h)\,dx_2 + \beta_1 \int \{N_k\} \nabla L(q_i^h)\,dx_2 + \beta_2 \int \nabla \{N_k\} L(\rho_0^h)\,dx_2 \equiv \{0\} \tag{19}$$

Upon definition of $k=1$ in Eq. (18), Eq. (19) represents a system of ordinary differential equations written on $x_l$. This system is converted to a nonlinear algebraic equation system, using the trapezoidal integration rule, and is solved using a Newton iteration algorithm.[13,14]

For the 2DPNS algorithm, the measure of continuity used to penalize the transverse momentum equation solution is defined as the solution to the Poisson equation,

$$L(\rho_0^h) \equiv \frac{d^2\phi^h}{dx_2^2} - \frac{\partial}{\partial x_j}(\tilde{u}_j^h) = 0 \tag{20}$$

subject to homogeneous Dirichlet boundary conditions at the freestream. The solution form for $\phi^h$ is given by Eq. (18), and the (finite element) algorithm statement is Eq. (19). In the limit of satisfaction of continuity, the solution to Eq. (20) becomes null, using an accumulation procedure during iteration as detailed in Ref. 12. The 2DPNS algorithm is equally applicable to the 2DBL problem specification by specifying a homogeneous Neumann boundary condition for $\phi$ at the airfoil surface. Similarly, the shear layer form of the 2DBL equation system could be used in the wake of a symmetric airfoil at zero angle of attack (only), assuming $\tilde{u}_2 \equiv 0$ and homogeneous Neumann boundary conditions for $\tilde{u}_1$, $k$, and $\epsilon$ on the wake symmetry plane. The developed 2DPNS system is required for nonsymmetric wake calculations.

## Physical Experiment

Validation of the accuracy of the theoretical model requires high quality experimental data for comparison. This experiment was conducted in the free-jet anechoic flow facility at NASA Langley Research Center. Figure 2 shows a top view of the test arrangement, including the symmetric NACA 63-012 airfoil section, with knife-sharp trailing edge, and the support for the subminiature cross hot-wire probe. The test conditions were selected as 0-deg angle of attack and a Reynolds number based on chord ($C$) of $1.2\times10^6$. The experimental data consist of mean and root mean square velocity distribution measured on traverses through the boundary layer and perpendicular to the wake centerline. Eight traverse stations lie on $0.9 \le x_1/C \le 0.9979$ and on $1.0029 \le x_1/C \le 1.10$, with close spacing in the immediate trailing edge vicinity. Figure 3 gives a composite plot of the experimental data upstream of the trailing edge, while Fig. 4 provides the data downstream. The measurement error in the streamwise velocity components is estimated less than 5%. For the transverse velocity components, and the shear stress, the estimated error is less than 10%. No pressure measurements were taken. A complete description of the experimental equipment and procedure is given in Ref. 15.

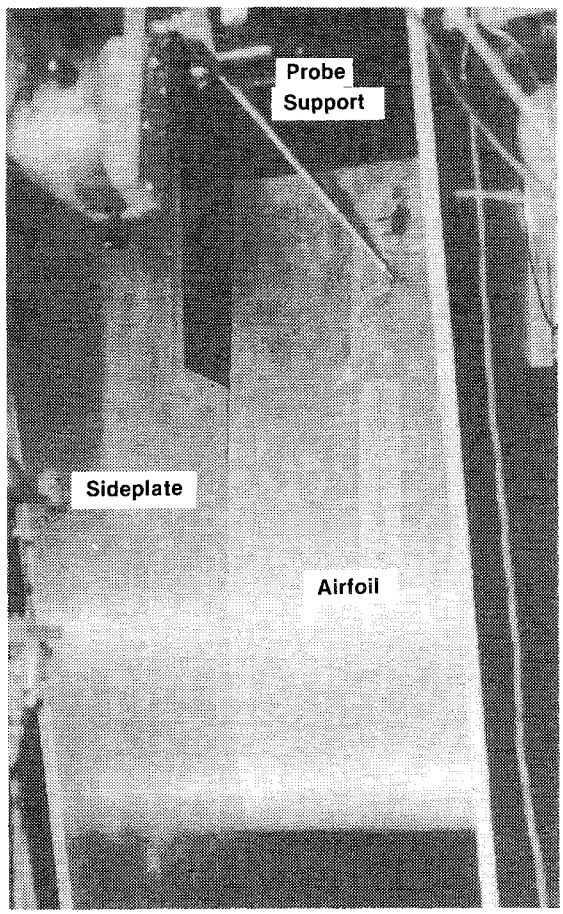


**Fig. 2 Top view of NACA 63-012 experimental configuration for boundary layer and wake measurements.**

## Computational Experiment

The viscous-inviscid numerical algorithm was evaluated for the experimental data case and for the same NACA 63-012 airfoil section at 6-deg angle of attack. The phase B viscous-corrected potential flow solution typically converged to four significant digits in $C_p(x_l)$ in five sweeps of airfoil thickness distribution augmentation by $\delta^*$.[7]

For the 0-deg data case, the experimental data profiles of $\tilde{u}_1$, $(\overline{u_1'u_1'})^{1/2} \equiv \tilde{u}_1'$, and $\overline{u_1'u_2'}$ were employed to initialize the 2DBL solution variable set at $x_1/C = 0.9$. Due to probe size restrictions, no data were measured on $0 \le x_2 \le 0.0005$ m, which corresponds to the interval $0 \le y^+ < 100$, where $y^+$ is the shear velocity Reynolds number.[6] Hence, a self-generation procedure was required developed for solution variable initiation in this region dominated by wall damping effects. Following some experimentation, a methodology was developed based upon Coles' law and mixing length theory that is extendible to self-generation of solution variable initialization throughout the entire boundary-layer region (in the absence of data). The dissipation length scale is assumed proportional to Prandtls' mixing length $l$ in the form,

$$l_d \equiv C^{-1/2}\omega^{\alpha} l \tag{21}$$

where $C$ and $\alpha$ are parameters to be determined. Since $\nu^t = \omega^{\beta} C_4 k^2/\epsilon$, then using Eq. (21)

$$k(x_1 = x_0, x_2) \equiv k_0 \equiv C\omega^{2(2-\alpha)} l^2 \left[\frac{\partial \tilde{u}_1}{\partial x_2}\right]^2 \tag{22}$$

since Coles' law has provided $\tilde{u}_1(x_2)$. Then using Eqs. (15) and (22)

$$\epsilon(x_1 = x_0, x_2) \equiv \epsilon_0 \equiv C^{1/2}\omega^{(\beta-\alpha)} C_4 k^{3/2} l^{-1} \tag{23}$$

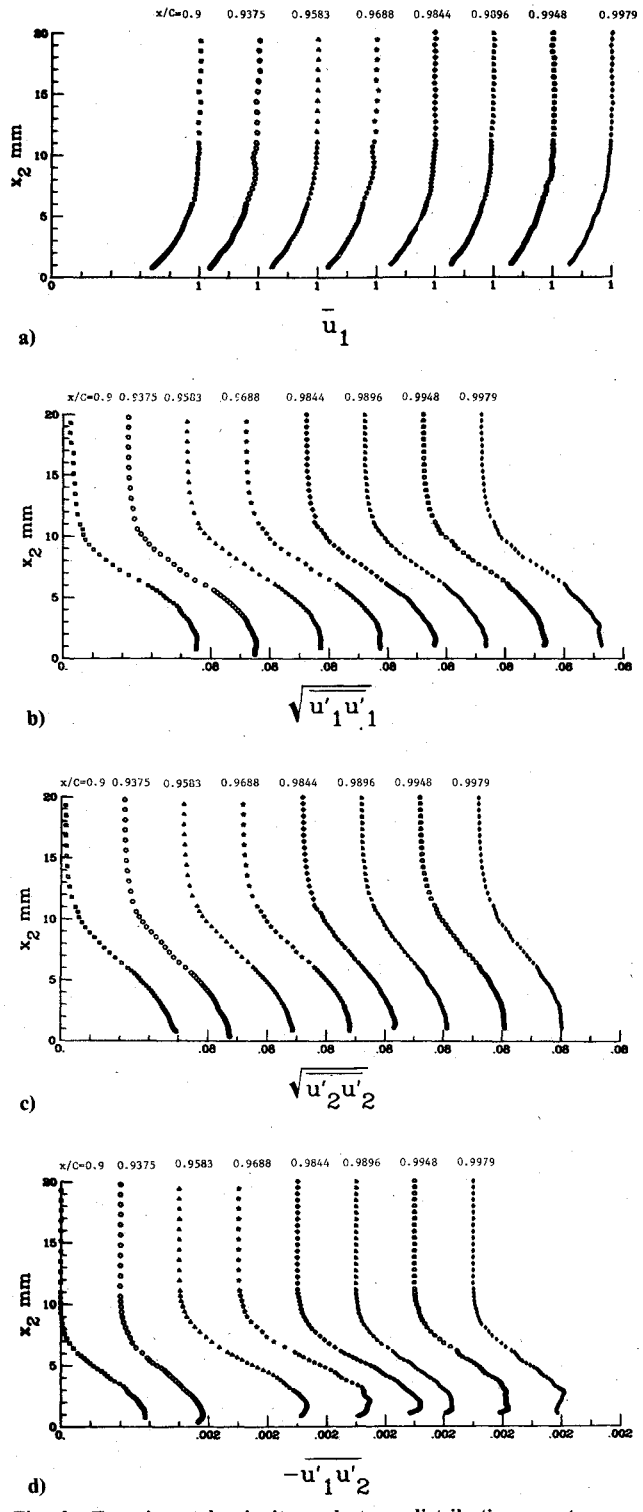


**Fig. 3 Experimental velocity and stress distributions upstream of trailing edge, $0.90 \le x_1/C \le 0.9979$, NACA 63-012, $\alpha = 0$ deg; a) mean velocity $\bar{u}_1$, b) Reynolds normal stress $\sqrt{\overline{u'_1 u'_1}}$, c) Reynolds normal stress $\sqrt{\overline{u'_2 u'_2}}$, and d) Reynolds shear stress $-\overline{u'_1 u'_2}$.**

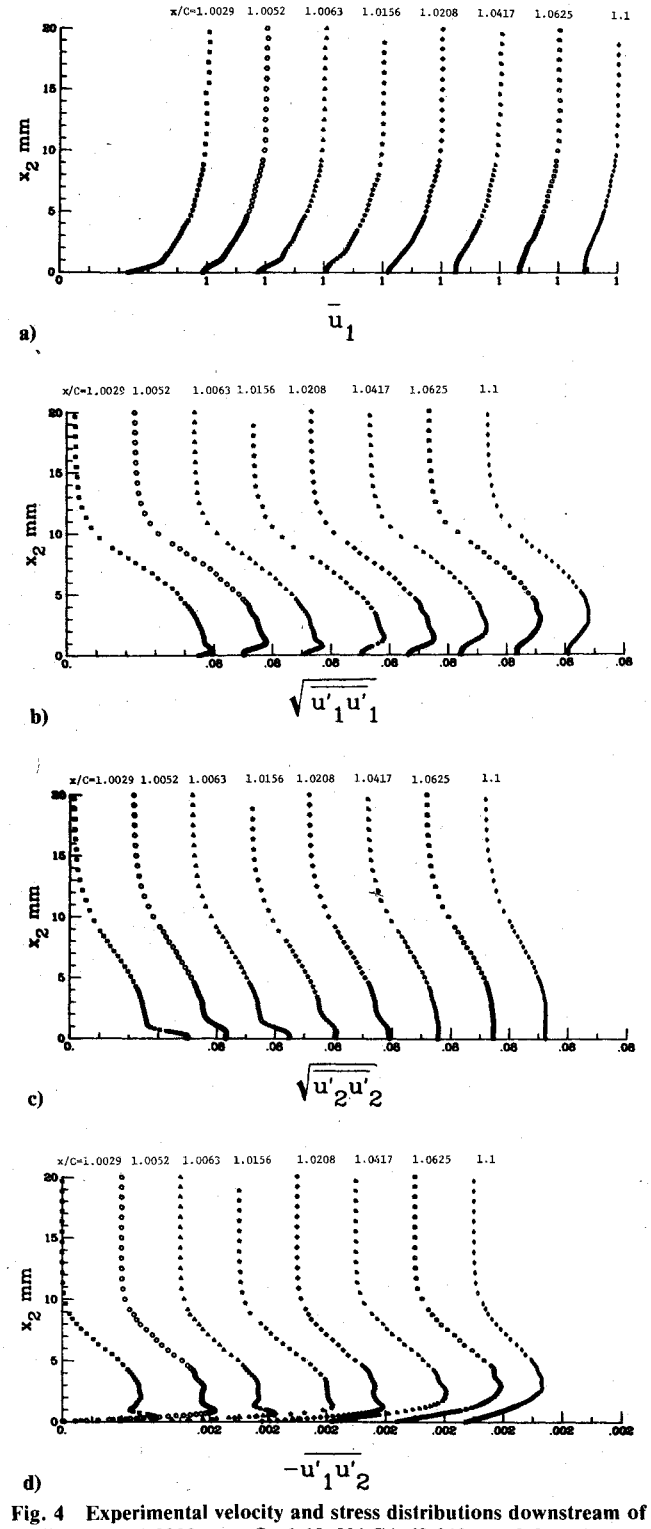


**Fig. 4 Experimental velocity and stress distributions downstream of trailing edge, $1.0029 \le x_1/C \le 1.10$, NACA 63-012, $\alpha = 0$ deg; a) mean velocity $\bar{u}_1$, b) Reynolds normal stress $\sqrt{\overline{u'_1 u'_1}}$, c) Reynolds normal stress $\sqrt{\overline{u'_2 u'_2}}$, and d) Reynolds shear stress $-\overline{u'_1 u'_2}$.**

Elsewhere, where the experimental data were available, the initial distributions were established assuming $\overline{u'_1} \approx \sqrt{C_1 k}$, i.e., neglecting the two other terms in $\overline{u'_1 u'_1}$, Eq. (13). Thus,

$$k_0 \equiv \overline{u'_1}^2 / C_1 \tag{24}$$

$$\epsilon_0 \equiv \omega^\beta C_4 k^{3/2} / l_d \tag{25}$$

$$l_d \ge \sqrt{C_1}\,\overline{u'_1 u'_2} \Big/ \left\{ \overline{u'_1} \left[ \frac{\partial \bar{u}_1}{\partial x_2} \right] \right\} \tag{26}$$

The form of Eq. (26) is selected to avoid division by products of small numbers. Hence, $l_d$ is defined a constant on $x_2/\delta > 0.9$ and both $k$ and $\epsilon$ may go to zero in the freestream. The results of numerical experimentation confirmed that $\alpha = 1.0$, $\beta = 2.0$, and $C = 3.0$ produced initial distributions that converged to solutions of Eqs. (2-6). Furthermore, selecting $\beta = 2.0$ and using the standard $k-\epsilon$ equation model constants ($C_k = 1.0$, $C_\epsilon = 1.3$, $C_\epsilon^1 = 1.44$, $C_\epsilon^2 = 1.92$) produced acceptable solution agreement with these data, as well as the Bradshaw relaxing boundary-layer flow data (IDENT 2400, Ref. 16).

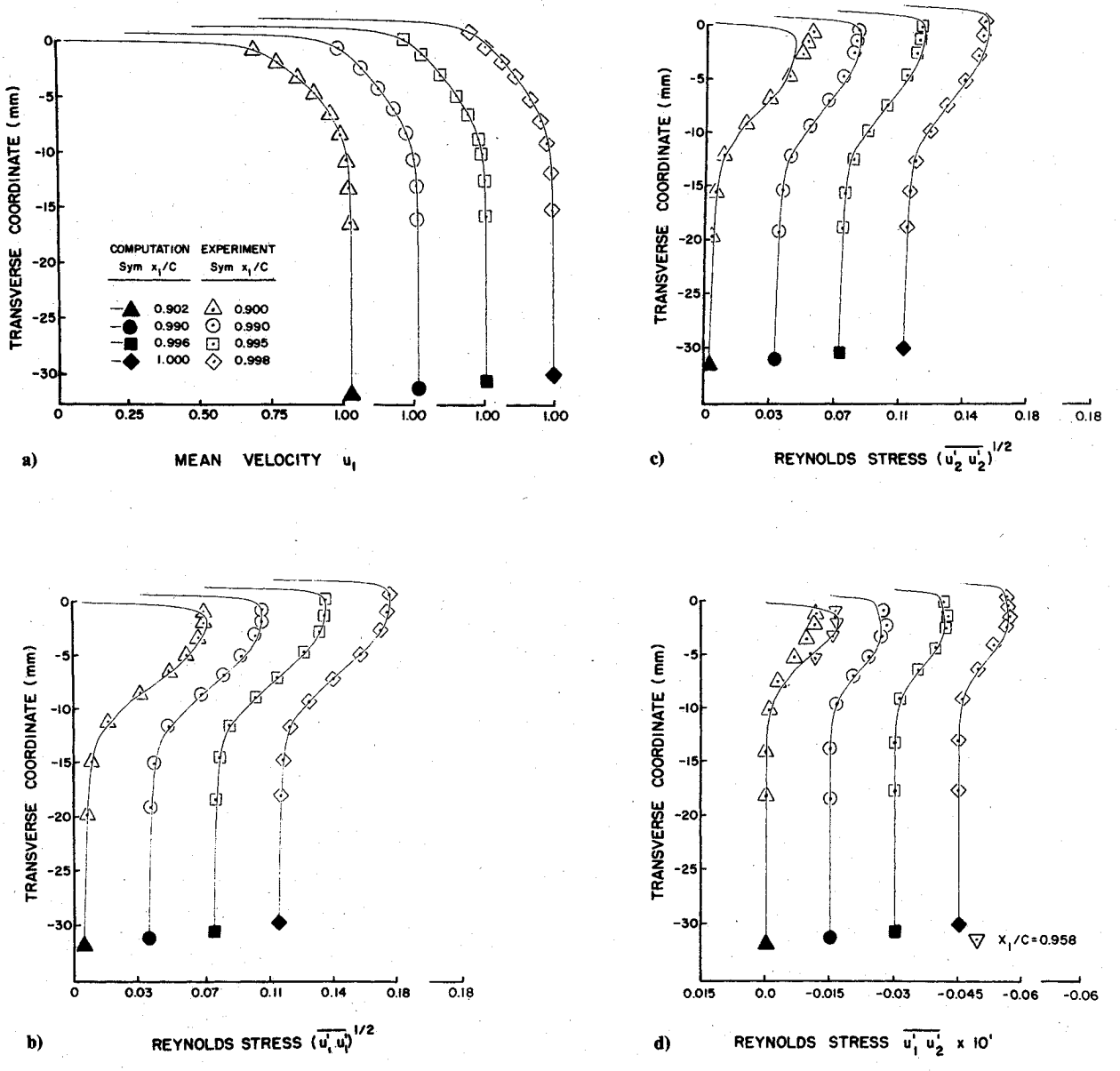


Fig. 5 Interaction algorithm 2DBL solution comparison to data, $0.902 \leq x_1/C \leq 1.000$, NACA 63-012, $\alpha = 0$ deg; a) mean velocity $\bar{u}_1$, b) Reynolds normal stress $\sqrt{\overline{u_1' u_1'}}$, c) Reynolds normal stress $\sqrt{\overline{u_2' u_2'}}$, and d) Reynolds shear stress $\overline{u_1' u_2'}$.

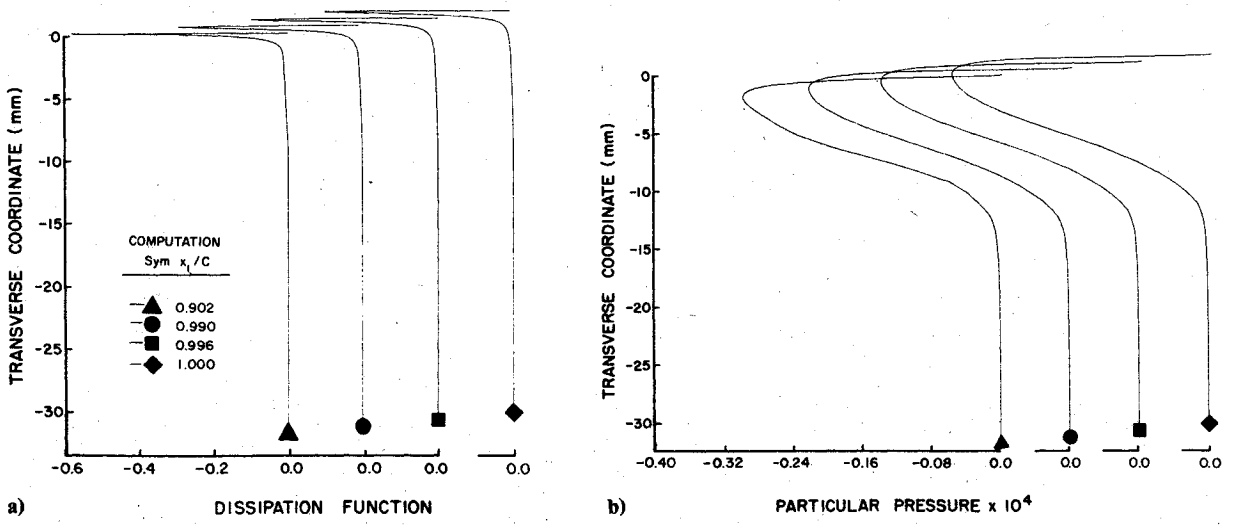


Fig. 6 Interaction algorithm 2DBL solution for dissipation and pressure particular solution, $0.9 \leq x_1/C \leq 1.0$, NACA 63-012, $\alpha = 0$ deg; a) dissipation function $\epsilon$ and b) pressure particular solution $p_p$.

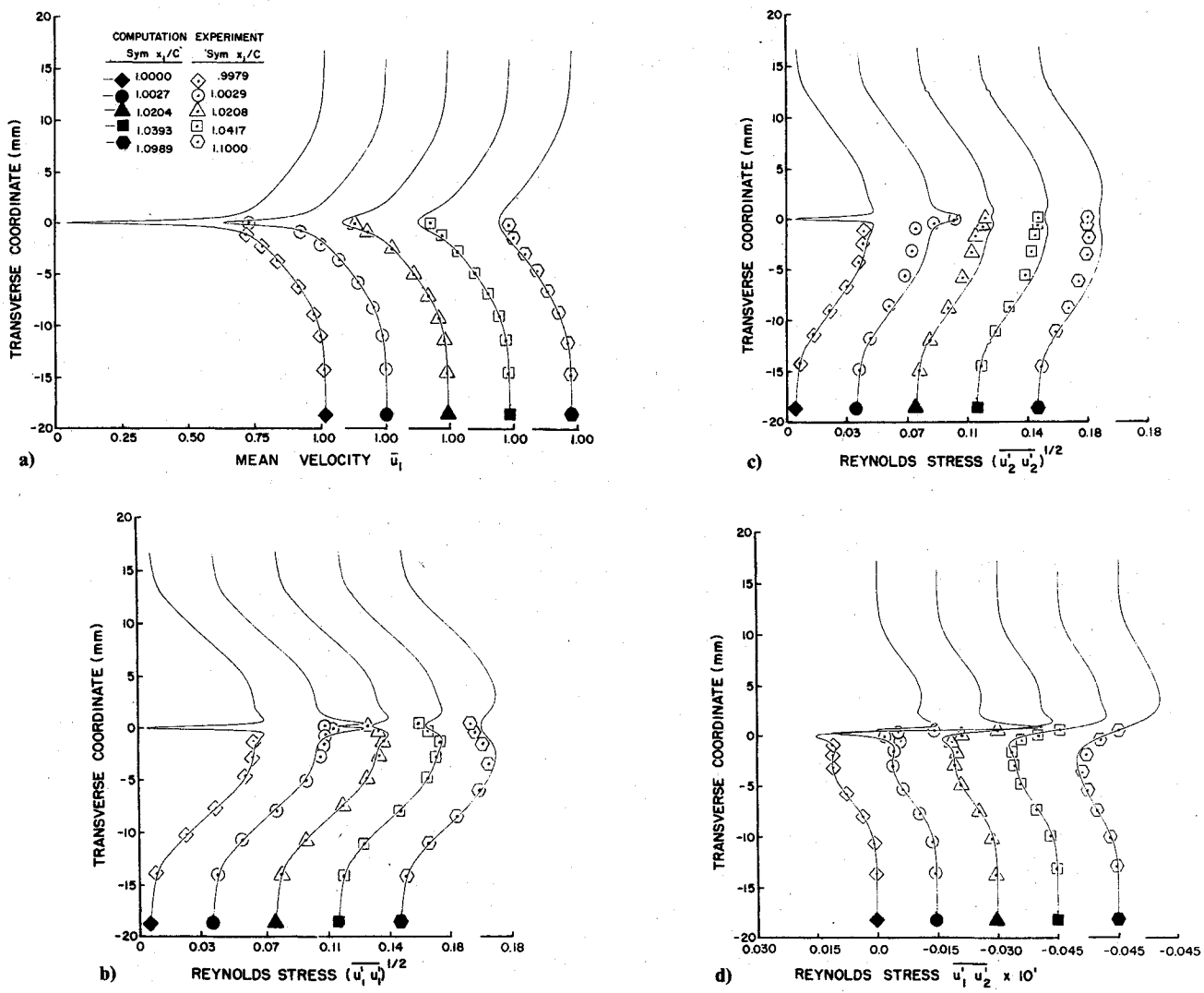


**Fig. 7 Interaction algorithm 2DPNS solution comparison to data, $1.0 \leq x_1/C \leq 1.10$, NACA 63-012, $\alpha = 0$ deg; a) mean velocity $\bar{u}_1$, b) Reynolds normal stress $\sqrt{u_1' u_1'}$, c) Reynolds shear stress $\sqrt{u_2' u_2'}$, and d) Reynolds shear stress $\overline{u_1' u_2'}$.**

Figure 5 summarizes the converged interaction algorithm 2DBL solution distributions for mean and fluctuating velocity correlation on the trailing edge region $0.9 < x_1/C \leq 1.0$. These data are oriented for flow on the airfoil underside, and each curve is shifted in plotting to avoid overlap. The symbols are select experimental data at the nearest station. The sole purpose in the 2DBL solution is to ensure that initialization of the wake computational experiment corresponds to the physical experiment to the maximum extent possible. The close agreement between data and the 2DBL solution confirms the high degree of compatibility achieved. The last three curves in each plot are the computational prediction over the last 1% chord, and are in excellent agreement with the data.

For reference, the first curve in each plot is the 2DBL solution at $x_1/C = 0.902$, which is seven integration steps downstream from solution initiation at $x_1/C = 0.899$. The agreement with the initializing experimental data (at $x_1/C = 0.9$) is excellent for $\bar{u}_1$ and $\overline{u_1' u_1'}$, as expected. The initial disparity between data and computation of $\overline{u_2' u_2'}$, at $x_1/C = 0.9$, is removed during the solution. Certain anomalies are apparent in the experimental data for $\overline{u_1' u_2'}$ on $0.93 \leq x_1/C \leq 0.96$, see Fig. 3d. The agreement between prediction and data at $x_1/C = 1.0$ was achieved by augmenting the initializing distribution $\overline{u_1' u_2'}$ by 50%, bringing it in close agreement with data at $x_1/C = 0.958$, as noted in Fig. 5d.

Figure 6 summarizes the 2DBL solution for dissipation function and particular (perturbation) pressure on $0.9 \leq x_1/C \leq 1.0$. The region where $\epsilon$ is highly spiked lies inside $y^+ \leq 30$, where the computation is essentially dominated by the low turbulence Reynolds number wall model. In distinction, the plots of $p_p$ are smooth in this region, hence also the turbulence kinetic energy distribution, see Eqs. (9) and (13). Repeating the 2DBL solution with a doubling of the computational grid refinement did not affect the solutions on the scale of plots in Figs. 5 and 6.

Figure 7 summarizes the converged interaction algorithm 2DPNS solution in the wake of the NACA 63-012 airfoil at zero angle of attack. The left curve in each plot is the 2DPNS solution at $x_1/C = 1.00002$, the first step solution. Sixty integration steps were taken to obtain the solution at $x_1/C = 1.0027$, the location of the first experimental data station. In comparison, only 130 integration steps were used to complete the 2DPNS solution on $1.0027 < x_1/C \leq 1.10$. The agreement between the data and the numerical prediction is generally excellent at all stations. The $\bar{u}_1$ minimum in the momentum defect region is underpredicted by 8% at $x_1/C = 1.0027$; this is reduced to 5% at $x_1/C = 1.10$, which is the experimental confidence. The computed spike in $\overline{u_1' u_1'}^{1/2}$ is sharper than data at $x_1/C = 1.0027$; thereafter, 2DPNS solution exhibits the double maxima and overall spreading rate of the data. At $x_1/C = 1.10$, the local minimum disparity with data is 9%. This may be the result of the larger sustained transverse gradients in $\bar{u}_1$. The same comparison is exhibited for $\overline{u_1' u_2'}$. The computed spike exceeds data by 60% at $x_1/C = 1.0027$; thereafter, overall agreement with peaks and spreading rate is generally excellent. The extremum shear

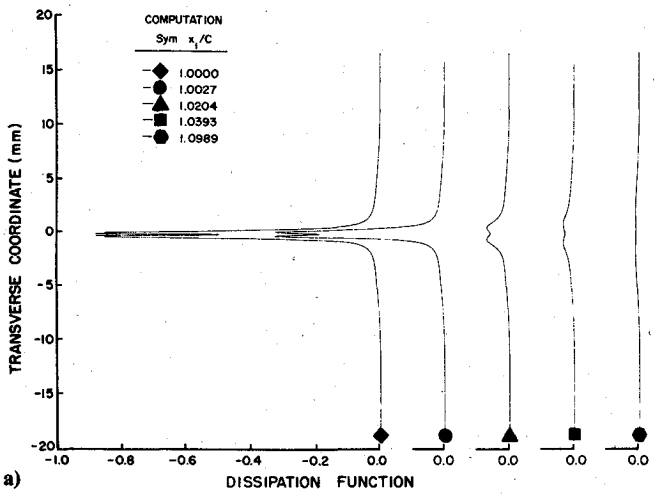


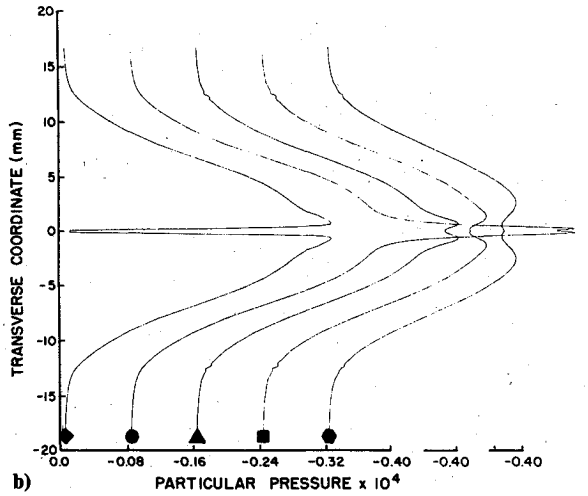


**Fig. 8 Interaction algorithm 2DPNS solution for dissipation and pressure particular solution, $1.0 \leq x_1/C \leq 1.10$, NACA 63-012, $\alpha = 0$ deg; a) dissipation function $\epsilon$ and b) pressure particular solution $p_p$.**

stress at $x_1/C = 1.10$ is underpredicted by 10%, which is the experimental confidence.

An anomaly exists in the experimental data for $\overline{u_2'u_2'}^{1/2}$, in that the overall level has decreased by about 30% compared with the upstream data. Hence, the numerical predictions lie above the data. Aside from this disparity, the computed spike at $x_1/C = 1.0027$ and the overall spreading and decay rates exhibit trends in good agreement with the data. In particular, the numerical prediction of a single extrema agrees with data, in marked distinction to the double extremum for $\overline{u_1'u_1'}^{1/2}$. This distinction in the computed stress profiles is due solely to the difference in sign of the third term in the tensor expansion for $\overline{u_k'u_k'}$, Eq. (13). The order of magnitude analysis indicates this term to be higher order, yet its significance is the major distinction in the normal stress distributions and confirmed by the experimental data.

Figure 8 summarizes the 2DPNS solution distribution for particular (perturbation) pressure and dissipation function. A large favorable $x_1$ pressure gradient is predicted in the momentum-defect core, between the trailing-edge terminus and $x_1/C = 1.0027$. Thereafter, it turns modestly adverse before essentially vanishing on $x_1/C > 1.02$. The initial zero level for $\epsilon$ on the wake centerline rapidly decreases in concert with reduction of the wall induced spike on $1.0 < x_1/C \leq 1.02$. Thereafter, dissipation function decays to a nominal null, but importantly nonzero distribution level.

Viewing these results, it is quite obvious that the consequential relaxation of the turbulent boundary layer is completed within the first fraction of a percent chord into the wake, i.e., $\Delta x_1/C \leq 0.003$. Even though a large particular pressure gradient was therein computed, its inclusion into the composite pressure field on the sequential algorithm passes increased $\bar{u}_1(x_1/C = 1.0027)$ only by about 2%, primarily due to the extremely short distance involved. Hence, the nearfield acceleration appears primarily responsive to the rate of turbulence mixing, coupled with the effects of continuity. Several computational experiments were executed wherein the length scale damping coefficient $\alpha$, Eq. (16), was decreased progressively on $0.99 \leq x_1/C \leq 1.0$, to sharpen the nearwall profiles of $\overline{u_i'u_j'}$ for initialization of the 2DPNS solution. The induced effects on the wake solution were indistinguishable on the scale of Fig. 7.

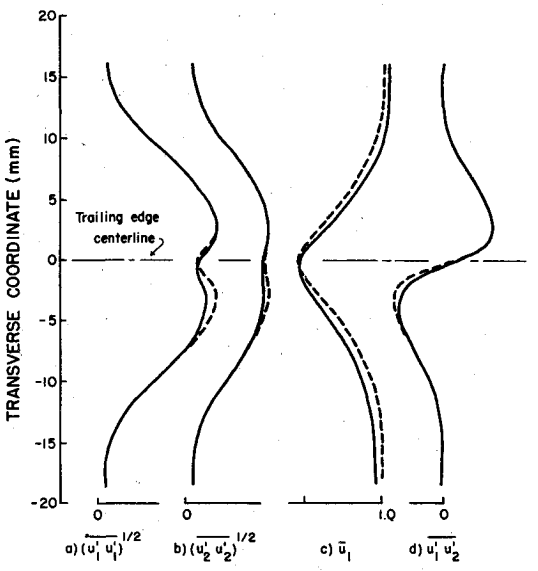


**Fig. 9 Comparison between 2DPNS solutions at $x_1/C = 1.10$, NACA 63-012, (----) $\alpha = 0$ deg and (—) $\alpha = 6$ deg; a) $\sqrt{\overline{u_1'u_1'}}$, b) $\sqrt{\overline{u_2'u_2'}}$, c) $\bar{u}_1$, and d) $\overline{u_1'u_2'}$.**

The 2DPNS solution does depend most critically on an initial condition specification that is a solution to the equation system, prior to extinction of the no-slip wall boundary condition. From this standpoint, the low turbulence Reynolds number model, permitting solution of the $k$ and $\epsilon$ equation through the sublayer region, was most crucial to the success of the computational experiment. With the confidence generated by the data comparison, the interaction algorithm can be applied to analysis on trailing-edge flows at nonzero angle of attack. While no experimental data are available for comparison, the computational predictions are comparable with themselves for trends. For example, Fig. 9 compares the computational experiment solution at $x_1/C = 1.10$ at $\alpha = 0$ and 6 deg. The nonsymmetries and level changes induced by angle of attack appear plausible, and are clear indicators of the trends to be expected in data from a physical experiment.

## Conclusions

A viscous-inviscid interaction algorithm is established for numerical prediction of two-dimensional aerodynamic flows in the wake of a sharp trailing edge airfoil. An essential algorithm element is a Reynolds stress closure model for use with solution of parabolized forms of the steady-flow, time-averaged Navier-Stokes equations. A coincident key development is identification and verification of a low turbulence Reynolds number model that permits solution of the parabolized two-equation closure system directly to the airfoil surface.

The turbulence model constants were set within the algorithm by comparison of numerical prediction with detailed experimental data in the trailing edge vicinity of a NACA 63-012 airfoil at zero angle of attack. The numerical predictions are in substantial agreement with the data,

especially with respect to generation and decay of Reynolds stress component peaks in the wake near field and distribution differences in the far field. The algorithm is equally applicable to nonseparated wake flow prediction at nonzero angle of attack.

By and large, the major problem encountered with the numerical algorithm was generation of acceptably accurate initial distributions of turbulence kinetic energy and dissipation function for the wake flow simulation. The primary requirement of the attached flow predictions before the trailing edge is to generate these initializations. Considerable effort was expended in developing a self-generation procedure, as necessitated by the lack of experimental data sufficiently close to the airfoil surface. Once accomplished, however, variation of parameters within the model exerted little influence on the flow predictions.

In summary, with the ultimate elimination of numerical and conceptual errors, the accuracy of the 2DBL/2DPNS wake flow prediction depends almost entirely on the initial distributions of the solution variables. In particular, for favorable comparison to physical data, it is imperative that the computational experiment accurately model the identical upstream flow configuration. Once established, the computational experiment can be exercised with confidence. The close association among the experimental and computational specialists, that was provided by this project, was singularly important in achieving the confirming results. It is the authors' consensus that this type of cooperation is of ultimate importance to the successful evolution of computational experimentation in turbulent aerodynamics.

## Acknowledgments

The computational phases of this project were supported principally by NASA Langley Research Center, under Contract NAS1-14855, with additional support under Contract NAS1-15105.

## References

[1] Bradshaw, P., "Prediction of the Turbulent Near Wake of a Symmetrical Airfoil," *AIAA Journal,* Vol. 8, Dec. 1970, p. 1507.

[2] Cebeci, T., Thiele, F., Williams, P. G., and Stewartson, K., "On the Calculation of Symmetric Wakes, I. Two-Dimensional Flows," *Journal of Numerical Heat Transfer,* Vol. 2, No. 1, 1979, pp. 35-60.

[3] Melnik, R. E. and Chow, R., "Asymptotic Theory of Two-Dimensional Trailing Edge Flows," NASA SP-347, 1975, pp. 177-249.

[4] Melnik, R. E. and Chow, R., "Turbulent Interaction at Trailing Edges," NASA CP-2001, 1976, pp. 1423-1425.

[5] Baker, A. J. and Manhardt, P. D., "Numerical Prediction of Mean and Fluctuating Velocities for Jet-Flap Flows," *AIAA Journal,* Vol. 16, Aug. 1978, pp. 807-814.

[6] Cebeci, T. and Smith, A. M. O., *Analysis of Turbulent Boundary Layers,* Academic Press, New York, 1974.

[7] Baker, A. J. and Orzechowski, J. A., "An Interaction Algorithm for Prediction of Mean and Fluctuating Velocities in Two-Dimensional Aerodynamic Wake Flows," NASA CR-3301, 1980.

[8] Lumley, J. L., "Toward A Turbulent Constitutive Relation," *Journal of Fluid Mechanics,* Vol. 41, Pt. 2, 1970, pp. 413-434.

[9] Gessner, F. B. and Emery, A. F., "A Reynolds Stress Model for Turbulent Corner Flows - Pt. 1: Development of the Model," *Transactions of ASME, Journal of Fluids Engineering,* June 1976, pp. 261-268.

[10] Launder, B. E., Reece, G. J., and Rodi, W., "Progress in the Development of a Reynolds-Stress Turbulence Closure," *Journal of Fluid Mechanics,* Vol. 68, Pt. 3, 1975, pp. 537-566.

[11] Hanjalic, K. and Launder, B. E., "A Reynolds Stress Model of Turbulence and its Application to Thin Shear Flows," *Journal of Fluid Mechanics,* Vol. 52, Pt. 4, 1972, pp. 609-638.

[12] Baker, A. J., "Research on Numerical Algorithms for the Three-Dimensional Navier-Stokes Equations, II. Dissipative Finite Element," USAF Rept. AFWAL-TR-80-3157, 1980.

[13] Soliman, M. O. and Baker, A. J., "Accuracy and Convergence of a Finite Element Algorithm for Laminar Boundary Layer Flow," *Computers and Fluids,* Vol. 9, March 1981, pp. 43-62.

[14] Soliman, M. O. and Baker, A. J., "Accuracy and Convergence of a Finite Element Algorithm for Turbulent Boundary Layer Flow," *Computer Methods in Applied Mechanics and Engineering,* 1981, to appear.

[15] Yu, J. C., "Mean Flow and Reynolds Stress Measurements in the Vicinity of the Trailing Edge of a NACA 63-012 Airfoil," NASA TP-1845, 1981.

[16] *AFOSR-IFP-Stanford Conference on Computation of Turbulent Boundary Layers - 1968,* Vol. I., edited by S. J. Kline, G. Sovran, M. V. Morkovan, and D. J. Cockrell; Vol. II, edited by D. A. Coles and E. A. Hirst, Stanford University, 1969.